Journal of the Mechanics and Physics of Solids 58 (2010) 1928–1946

Contents lists available at ScienceDirect

Journal of the Mechanics and Physics of Solids

journal homepage: www.elsevier.com/locate/jmps

A two-scale time-dependent damage model based on non-planar growth of micro-cracks

Bertrand François [a,b], Cristian Dascalu [c,*]

[a] FRS-FNRS – Fonds National de la Recherche Scientifique, rue d'Egmont 5, B-1000 Bruxelles, Belgium
[b] Université de Liège, Department ArGEnCo, Chemin des Chevreuils 1, 4000 Liège 1, Belgium
[c] Laboratoire Sols Solides Structures - Risques, UJF, INPG, CNRS UMR 5521, Domaine Universitaire, B.P. 53, 38041 Grenoble cedex 9, France

ARTICLE INFO

Article history:
Received 18 December 2009
Received in revised form
21 June 2010
Accepted 23 July 2010

Keywords:
Subcritical propagation
Crack rotation
Homogenization
Time-dependent damage
Size effects

ABSTRACT

This paper presents the theoretical developments and the numerical applications of a time-dependent damage law. This law is deduced from considerations at the micro-scale where non-planar growth of micro-cracks, following a subcritical propagation criterion, is assumed. The orientation of the crack growth is governed by the maximum energy release rate at the crack tips and the introduction of an equivalent straight crack. The passage from micro-scale to macro-scale is done through an asymptotic homogenization approach. The model is built in two steps. First, the effective coefficients are calculated at the micro-scale in finite periodical cells, with respect to the micro-cracks length and their orientation. Then, a subcritical damage law is developed in order to establish the evolution of damage. This damage law is obtained as a differential equation depending on the microscopic stress intensity factors, which are *a priori* calculated for different crack lengths and orientations. The developed model enables to reproduce not only the classical short-term stress–strain response of materials (in tension and compression) but also the long-term behavior encountering relaxation and creep effects. Numerical simulations show the ability of the developed model to reproduce this time-dependent damage response of materials.

1. Introduction

In many engineering applications, the damage evolution of materials must be accurately considered. The modeling of the nucleation and the growth of micro-cracks in solids due to various mechanical loadings is of particular interest in order to assess the stress–strain behavior of damaged materials. As long as micro-cracks propagate, the overall stiffness of materials may drastically decrease and provoke failure when coalescence of adjacent micro-cracks occurs.

At micro-scale, materials contain various sources of heterogeneities such as cracks, pores, inclusions or grain boundaries. In particular, the presence of such flaws strongly affects the macroscopic mechanical behavior of materials by serving as stress concentrators and leading to the formation of micro-cracks. In many materials, the micro-crack distribution may be locally approximated by a periodic one. This periodic structure is characterized by an internal length, that is the distance between two adjacent micro-cracks. Since the consideration of a large number of cracks in the material is difficult, in the construction of a constitutive model a more efficient method is to determine a mechanically equivalent homogeneous material at the macro-scale, having relatively similar properties than the heterogeneous medium. Within this framework, the macroscopic description

* Corresponding author. Tel.: +33 4 76 82 70 82; fax: +33 4 76 82 70 00.
E-mail address: Cristian.Dascalu@hmg.inpg.fr (C. Dascalu).

0022-5096/$ - see front matter © 2010 Elsevier Ltd. All rights reserved.
doi:10.1016/j.jmps.2010.07.018

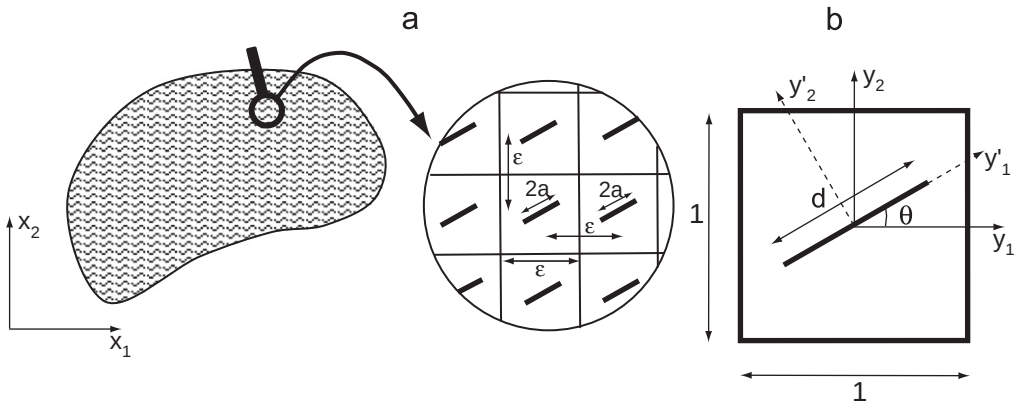

Fig. 1. (a) Fissured medium with locally periodic micro-structure. (b) Unit cell with rescaled crack of length d. $2a$: length of the micro-crack, ε: distance between two adjacent micro-cracks (internal length), θ: orientation of the micro-crack with respect to the y_1-axis.

can be obtained by phenomenological approach, directly at the macroscopic scale through continuum damage models (e.g. Dragon and Mroz, 1979; Chaboche, 1992; Voyiadjis and Park, 1999; Carol et al., 2001) or by homogenization procedures (Andrieux et al., 1986; Lene, 1986; Nemat-Nasser and Horii, 1993; Dascalu et al., 2008; Zhu et al., 2008; Dartois et al., 2009). An approach by homogenization is used in the present work (Fig. 1a), the behavior of the macroscopic structure being deduced from the properties of the material at the micro-scale. The stiffness of the solid is governed by homogenized coefficients that depend on the elastic properties of the solid matrix, the lengths and the orientations of micro-cracks (Wang et al., 2000; Wang, 2005; Kachanov, 2007). The orientation of micro-cracks induces the anisotropy in the global response of the material.

The evolution of damage in many materials, such as glasses, rocks, ceramics or ceramic composites, is time-dependent. An important source of time-dependency is the subcritical propagation of micro-cracks. The classical criteria of crack propagation, such as the Griffith (1921) criterion, ignore the time effect on the fracture behavior. On the contrary, a subcritical criterion, that is a criterion considering crack propagation for energy lower than the critical limit of fracture, takes into account time effects (Anderson and Grew, 1977; Atkinson and Meredith, 1987). At the micro-scale, the tensile failure due to the subcritical propagation of cracks may be the dominant effect of creep observed at the macro-scale, even under macroscopically compressive stress fields. The rate of crack propagation may be expressed with respect to stress intensity factor at the crack tips, under tensile mode, with a power law (Charles, 1958) or an exponential law (Wiederhorn and Bolz, 1970). The first one will be used in this study.

In the present work, the stress–strain evolution is governed by a subcritical damage law that accounts for the non-planar growth of micro-cracks. We consider that kinking of micro-cracks occurs in the direction that maximizes the energy release rate. The damage evolution of the material is related to the formation of open tension micro-cracks which can be produced by both globally tensile or compressive stress fields. At each time step, the propagation of the open tension micro-crack produces an out-of-plane extension of the crack. Then, the obtained kinked crack is replaced, at each time step, by an equivalent crack. This model is an efficient alternative to the well-established models of "wing" crack propagations (Nemat-Nasser and Horii, 1982; Horii and Nemat-Nasser, 1985; Lauterbach and Gross, 1998; Paliwal and Ramesh, 2008; Schulson, 2001; Huang and Subhash, 2003). A different view has been taken by Bhattacharya et al. (1998) who proposed an energy-based model of compressive splitting in heterogeneous brittle solids. A stochastic damage model, based on macro-crack–micro-crack interaction, was proposed by Lua et al. (1992a, 1992b) in order to quantify the inherent statistical distribution of the fracture toughness of multi-phase brittle materials. Assuming also non-planar growth of cracks, Liu et al. (1996) solved fatigue crack reliability problems by considering the curvilinear crack propagation as a stochastic process governed in length and in orientation by statistical laws.

Also, the non-planar crack propagation is affected by the interaction between micro-cracks. Several approximate numerical methods have been developed to deal with interacting micro-cracks such as the complex potentials (Muskhelishvili, 1953), the boundary integral equation approach (Hu and Chandra, 1993; Dong and Lee, 2005) or the method of pseudo-tractions (Horii and Nemat-Nasser, 1985; Karihaloo and Wang, 1997). However, it is generally unrealistic to account for the mutual effects of each crack between each others by superposing the interaction of the stress fields. In that context, the asymptotic homogenization (Sanchez-Palencia, 1980; Leguillon and Sanchez-Palencia, 1982) provides an efficient mathematical framework to overcome such a limitation. The homogenized coefficients are calculated on a unit cell with a single crack and periodic boundary conditions. So, the interaction between adjacent micro-cracks is implicitly considered by the assumption of local periodicity of the micro-structure.

Using a micromechanics-based approach, the model characterizes the nucleation and the propagation of damage. A general two-scale approach for damage, including subcritical evolution as a particular case, was described in Dascalu (2009), generalizing previous works (Dascalu and Bilbie, 2007; Dascalu et al., 2008) on brittle damage. Here we develop the subcritical damage model and we extend the assumption of planar propagation toward the consideration of crack rotation.

The paper is organized as follows. First, the mathematical formulation of the model, including the macroscopic equilibrium equations, the asymptotic homogenization procedure and the subcritical propagation of cracks, is presented. The next section addresses the calculation of the stress intensity factors that are needed to quantify the subcritical growth of cracks at the tips. Then, the procedure to replace the kinked crack by an equivalent straight crack is explained. Finally, the model is validated by means of numerical examples, emphasizing the time-dependent response of materials.

2. Mathematical formulation

Consider a two-dimensional isotropic elastic medium containing a locally periodic distribution of micro-cracks. Each crack is straight with a length $2a$ and an orientation of angle θ with respect to the x_1 direction (abscissa of the referential system considered at the macro-scale). The length $2a$ and the orientation θ are assumed to vary smoothly almost everywhere in the elastic body. The damage variable d, varying between 0 (for virgin material) and $1/[\max(|\cos(\theta)|;|\sin(\theta)|)]$ (for cell completely crossed by the micro-crack), is the ratio between the crack length $2a$ and the distance between two micro-cracks ε:

$$d=\frac{2a}{\varepsilon} \tag{1}$$

The length ε also represents the size of the periodicity cell (Fig. 1).

2.1. Equilibrium equations

In the solid part $\mathcal{B}_s=\mathcal{B}\backslash\mathcal{C}$, where $\mathcal{B}$ is the whole body and $\mathcal{C}$ the union of all the micro-cracks in $\mathcal{B}$, the momentum equilibrium is

$$\frac{\partial\sigma_{ij}^{\varepsilon}}{\partial x_j}=0 \quad \text{in } \mathcal{B}_s \tag{2}$$

and the linear elasticity constitutive relation is

$$\sigma_{ij}^{\varepsilon}=a_{ijkl}e_{xkl}(\mathbf{u}^{\varepsilon}) \tag{3}$$

where a_{ijkl} is the elasticity tensor. $\sigma_{ij}^{\varepsilon}$ is the stress field and $\mathbf{u}^{\varepsilon}$ the displacement field from which the strain tensor is deduced in the small deformation hypothesis

$$e_{xij}(\mathbf{u}^{\varepsilon})=\frac{1}{2}\left(\frac{\partial u_i^{\varepsilon}}{\partial x_j}+\frac{\partial u_j^{\varepsilon}}{\partial x_i}\right) \tag{4}$$

On the crack faces, traction free opening or frictionless contact conditions are assumed. These two alternatives are respectively expressed by the two sets of formulae

$$\boldsymbol{\sigma}^{\varepsilon}\mathbf{N}=0, \quad [\mathbf{u}^{\varepsilon}\cdot\mathbf{N}]>0 \tag{5}$$

$$[\boldsymbol{\sigma}^{\varepsilon}\mathbf{N}]=0, \quad \mathbf{N}\cdot\boldsymbol{\sigma}^{\varepsilon}\mathbf{N}<0, \quad \mathbf{T}\cdot\boldsymbol{\sigma}^{\varepsilon}\mathbf{N}=0, \quad [\mathbf{u}^{\varepsilon}\cdot\mathbf{N}]=0 \tag{6}$$

where $\mathbf{N}$ is the unit normal vector, $\mathbf{T}$ is a unit tangent vector to the crack and $[\cdot]$ the jump across the crack. For each micro-crack, we assume that one of the two states (5) and (6) holds in all the crack points. The fact that each micro-crack is completely open or closed is a reasonable assumption for small crack lengths. The way in which the switch from one state to the other is controlled will be described later, in terms of the homogenized solution (Eq. (17)).

2.2. Asymptotic homogenization

The locally periodic micro-structure is constructed from a unit cell Y which includes the set of points in the orthogonal axis system (y_1, y_2) centered in the middle of the crack, such that $y_1\in[-0.5,0.5]$ and $y_2\in[-0.5,0.5]$. The crack is rotated with an angle θ with respect to y_1-axis. A second axis system (y'_1,y'_2), rotated with an angle θ with respect to (y_1, y_2), is attached to the crack. Then this unit cell is rescaled by the parameter ε so that the period of the material is εY (Fig. 1b). We assume that the micro-structural length ε is small enough with respect to the characteristic dimension of the solid body, so that to distinguish between microscopic and macroscopic variations. Within this two-scale framework, the two distinct scales are represented by the variable $\mathbf{x}$, which is referred to as macroscopic variable and the variable $\mathbf{y}=\mathbf{x}/\varepsilon$, referred to as microscopic variable (Sanchez-Palencia, 1980; Leguillon and Sanchez-Palencia, 1982).

The unit cell Y contains the crack CY and $Y_s=Y\backslash CY$ is the solid part. Following the method of asymptotic homogenization (e.g. Benssousan et al., 1978; Sanchez-Palencia, 1980), we look for expansions of $\mathbf{u}^{\varepsilon}$ and $\boldsymbol{\sigma}^{\varepsilon}$ in the form

$$\mathbf{u}^{\varepsilon}(\mathbf{x},t)=\mathbf{u}^{(0)}(\mathbf{x},\mathbf{y},t)+\varepsilon\mathbf{u}^{(1)}(\mathbf{x},\mathbf{y},t)+\varepsilon^2\mathbf{u}^{(2)}(\mathbf{x},\mathbf{y},t)+\cdots \tag{7}$$

$$\boldsymbol{\sigma}^{\varepsilon}(\mathbf{x},t)=\frac{1}{\varepsilon}\boldsymbol{\sigma}^{(-1)}(\mathbf{x},\mathbf{y},t)+\boldsymbol{\sigma}^{(0)}(\mathbf{x},\mathbf{y},t)+\varepsilon\boldsymbol{\sigma}^{(1)}(\mathbf{x},\mathbf{y},t)+\cdots \tag{8}$$

where $\mathbf{u}^{(i)}(\mathbf{x},\mathbf{y},t),\boldsymbol{\sigma}^{(i)}(\mathbf{x},\mathbf{y},t),\mathbf{x}\in\mathcal{B}_s,\mathbf{y}\in Y$ are smooth functions and Y-periodic in $\mathbf{y}$.

Based on the previous works (e.g. Leguillon and Sanchez-Palencia, 1982; Dascalu et al., 2008), we can show that the substitution of Eqs. (7) and (8) in the set of expressions (2)–(6), gives the following relationships for different order of ε. At zero order of ε

$$\frac{\partial}{\partial y_j}(a_{ijkl}e_{ykl}(\mathbf{u}^{(0)})) = 0 \quad \text{in } Y_s \tag{9}$$

$$(a_{ijkl}e_{ykl}(\mathbf{u}^{(0)}))N_j = 0 \quad \text{on } CY^{\pm} \tag{10}$$

where e_{ykl} is the microscopic strain, calculated with respect to $\mathbf{y}$ variables.

Based on the assumption of separation of scales, the variables $\mathbf{x}$ and $\mathbf{y}$ are considered as independent. The coefficients a_{ijkl} being assumed constant in the unit cell, Eq. (9) shows that the displacement $\mathbf{u}^{(0)}=\mathbf{u}^{(0)}(\mathbf{x},\mathbf{t})$ does not depend on $\mathbf{y}$, being the true macroscopic displacement.

The problem for the first order of ε is obtained as

$$\frac{\partial}{\partial y_j}(a_{ijkl}e_{ykl}(\mathbf{u}^{(1)})) = 0 \quad \text{in } Y_s \tag{11}$$

$$a_{ijkl}e_{ykl}(\mathbf{u}^{(1)})N_j = -a_{ijkl}e_{xkl}(\mathbf{u}^{(0)})N_j \quad \text{on } CY^{\pm} \tag{12}$$

with periodicity conditions on the cell boundary. The first-order corrector $\mathbf{u}^{(1)}$ plays the role of microscopic displacement and will contribute to the effective coefficients, as shown below.

For the overall response, we deduce

$$\frac{\partial}{\partial x_j}\Sigma_{ij}^{(0)} = 0 \tag{13}$$

where

$$\Sigma_{ij}^{(0)} = C_{ijkl}e_{xkl}(\mathbf{u}^{(0)}) \tag{14}$$

$$C_{ijkl}^{\pm}(d,\theta) = \frac{1}{|Y|}\int_{Y_s}(a_{ijkl} + a_{ijmn}e_{ymn}(\xi_{\pm}^{kl}))\,dy \tag{15}$$

are the macroscopic stress and the homogenized coefficients, respectively. Eq. (13) is the homogenized equation of equilibrium. In each regime (opening or closure), we can prove that the microscopic correction $\mathbf{u}^{(1)}$ is

$$\mathbf{u}_{\pm}^{(1)} = \xi_{\pm}^{pq}\,e_{xpq}(\mathbf{u}^{(0)}) \tag{16}$$

where $\xi_{\pm}^{pq}$ are elementary solutions of (11)–(12) for particular $e_{xpq}(\mathbf{u}^{(0)})$ (Leguillon and Sanchez-Palencia, 1982; Dascalu et al., 2008). The distinction $\pm$ corresponds to opening (+) or contact (−) conditions of the crack lips. The difference between these microscopic states of contact and opening are obtained from the orientation of the force vector, deduced from the force-type source term of Eq. (12), with respect to crack line. In the space of macroscopic deformations, these two states induce a separation of the space $\mathbf{R}$ of deformations e_{x11}, e_{x12}, e_{x22} into two subregions $\mathbf{R}^{\pm}$ defined by

$$\mathbf{R}^{\pm} = \{\mathbf{e}_{\mathbf{x}} |\ N_i a_{ijkl}e_{xkl}(\mathbf{u}^{(0)})N_j \gtrless 0\} \tag{17}$$

The homogenized coefficients C_{ijkl} depend on the state of damage of the material (i.e. d and θ) and on the mechanical properties of the solid matrix. For an isotropic matrix, characterized by the Young modulus E and the Poisson ratio ν (for simulations we consider $E=2$ GPa and $\nu=0.3$), the coefficients can be initially computed for a large number of $d^{\star} \in [0,1]$ ($d^{\star} = d/\max(|\cos(\theta)|;|\sin(\theta)|)$ being the normalized damage variable) and $\theta \in [0^{\circ},180^{\circ}]$ and for both states of tension or compression, obtaining in this way, after interpolation, polynomial expressions of $C_{ijkl}(d,\theta)$. This is done using the solution of the unit cell problem (11)–(12) (Dascalu et al., 2008). Then, the homogenized coefficients are calculated from the obtained strain field $e_{ymn}(\xi^{kl})$ through the integral (15).

The presence of micro-cracks induces anisotropy in the effective behavior. It can be shown that the usual symmetries hold for the homogenized coefficients: $C_{ijkl} = C_{jikl} = C_{ijlk} = C_{jilk}$. So that, the following different coefficients have to be determined in each regime: C_{1111}, C_{2222}, C_{1122}, C_{1212}, C_{1112}, C_{2212}. For different values of d and θ, each of the 12 coefficients (six in tensile mode and six in compressive mode) is obtained by linear interpolation between the polynomial curves presented in Figs. 2 and 3.

2.3. Subcritical growth of micro-cracks

The evolution of the micro-crack length during propagation is described through a subcritical criterion adapted from the Charles' (1958) law as used by many authors (Miura et al., 2003; Main, 2000; Kemeny, 2005, among others)

$$\frac{dl}{dt} = v_0\left(\frac{K_I^{\star}}{K_0}\right)^n \tag{18}$$

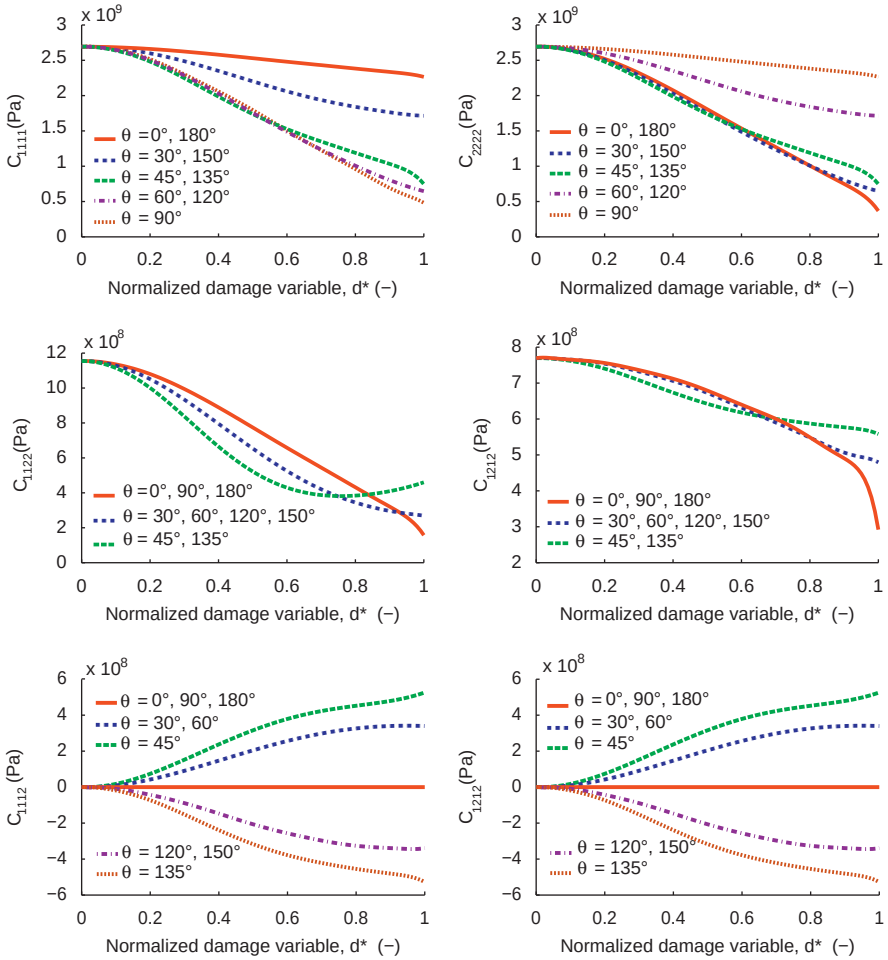

Fig. 2. Evolution of the homogenized coefficients with respect to the normalized damage variable d and the crack orientation θ: opening conditions of the crack lips ($\mathbf{R}^+$ domain).

where v_0 is a referential velocity of crack propagation and n is the subcritical growth coefficient. $K_I^\star$ is the stress intensity factor for the tensile mode of rupture (Mode I). This criterion is used to describe the propagation of the kinked crack (Fig. 4) and the corresponding stress intensity factor is indicated by the star upper index. K_0 is a particular stress intensity factor for which the velocity of the crack propagation is equal to v_0. K_0, v_0 and n are material parameters. $K_I^\star$ depends on the stress state, the internal length ε and the geometry of the micro-cracks. The determination of this stress intensity factor is explained in the next section.

The crack is assumed to propagate in the direction that maximizes the energy release rate. This criterion produces a kinking angle between the existing crack and the incrementally propagated crack (Fig. 4). This kinking angle can be expressed with the following function (Schütte and Bruhns, 2002):

$$\phi_{max} = \mathrm{sgn}(K_{II})[0.70966\lambda^3 - 0.097725\sin^2(3.9174\lambda) - 13.1588\tanh(0.15199\lambda)] \tag{19}$$

where sgn is the signum function and λ is a mode mixity factor that combines the stress intensity factors of mode I, K_I, and mode II, K_{II}, of the straight crack:

$$\lambda = \frac{|K_{II}|}{K_I + |K_{II}|} \tag{20}$$

So, at the level of the crack tips, the propagation of the kinked crack is governed in length and orientation by Eqs. (18) and (19), respectively. The question of how to determine the stress intensity factors K_I and K_{II} of the straight micro-crack and $K_I^\star$ of the kinked crack is addressed in the next section.

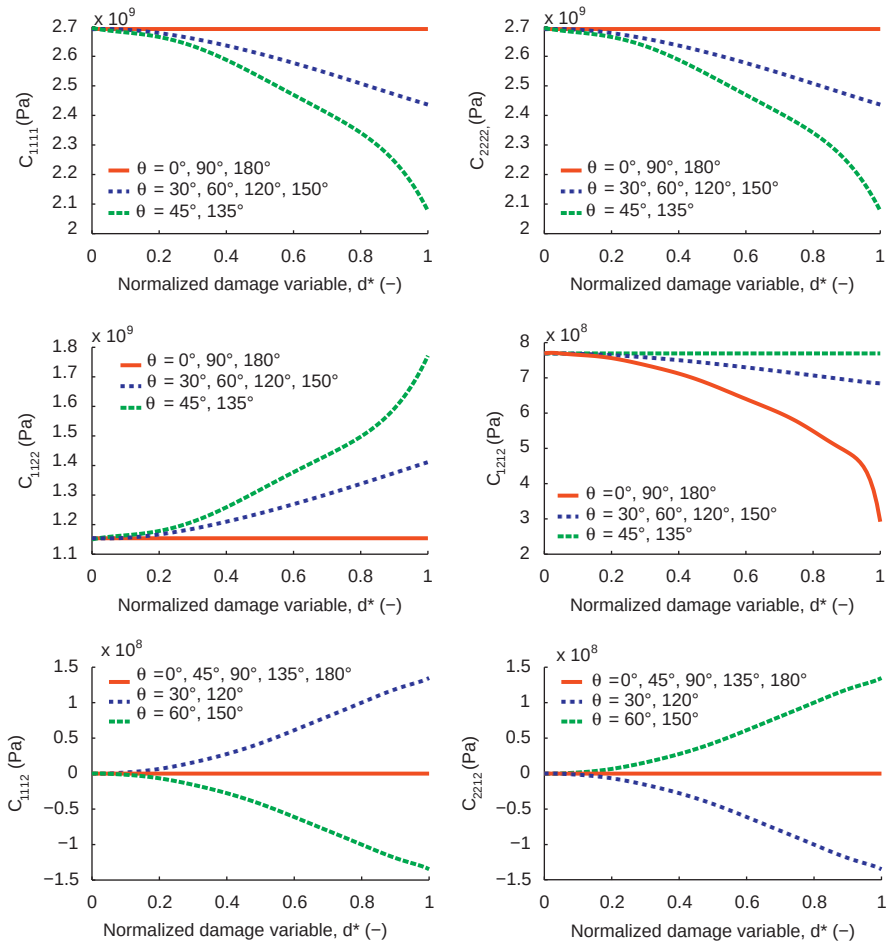

Fig. 3. Evolution of the homogenized coefficients with respect to the normalized damage variable d and the crack orientation θ: contact conditions of the crack lips ($\mathbf{R}^-$ domain).

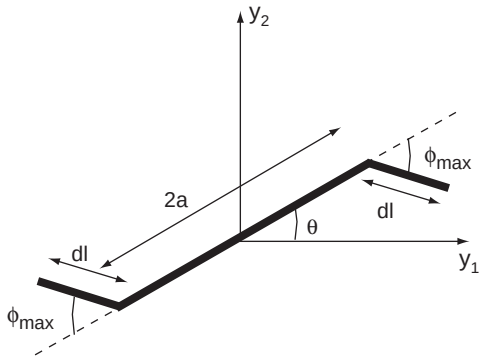

Fig. 4. Kinked crack. The out-of-plane crack growth propagates in the direction that maximize the energy release rate. ϕ_{max} is the angle between the crack line and the crack extension.

3. Stress intensity factors

3.1. Straight cracks

Specific techniques are generally required for the determination of the stress intensity factors K_I and K_{II}. Analytical expressions may be obtained for standard cases, such as a finite crack or a one-dimensional array of finite cracks in an

infinite body. Also, some practical problems have been calculated in the past and tabulated in stress intensity factors handbooks (Murakami and Aoki, 1987; Tada et al., 2000). For a single mode of crack loading (exclusively mode I or exclusively mode II), the non-null stress intensity factor can be deduced from the energy release rate at the crack tips $\mathcal{G}^\varepsilon$ (in a plane strain configuration):

$$\mathcal{G}^\varepsilon = \frac{1-\nu^2}{E}[K_{\mathrm{I}}^2 + K_{\mathrm{II}}^2] \tag{21}$$

under the condition that K_{I} or K_{II} is null.

Based on micro-mechanical energy balance on a periodicity cell with evolving micro-cracks and assuming a straight micro-crack trajectory and a traction-free opening (Eq. (5)) or frictionless contact of the crack lips (Eq. (6)), Dascalu et al. (2008) deduced the following energy balance equation entirely expressed in terms of the homogenized solution $\mathbf{u}^{(0)}$, that enables to determine the energy release rate $\mathcal{G}^\varepsilon$ for the locally periodic structure:

$$\frac{dd}{dt}\left(\frac{1}{2}\frac{\partial C_{ijkl}(d,\theta)}{\partial d}e_{xkl}(\mathbf{u}^{(0)})e_{xij}(\mathbf{u}^{(0)}) + \frac{\mathcal{G}^\varepsilon}{\varepsilon}\right) = 0 \tag{22}$$

The first term in the parenthesis is the negative of the damage energy release rate. For evolving damage, the previous relation shows that the micro-structural length ε makes the link between the surface energy dissipated during micro-crack propagation and damage energy dissipated per unit volume.

This relation has been employed in Dascalu et al. (2010) to obtain a two-scale time-dependent damage model for straight propagation of micro-cracks. However, if mixed modes of crack loading are considered, individual stress intensity factor modes cannot be determined from the energy-release rate and a different technique must be used. Such techniques generally include local computations at the crack tips or use of path-independent integrals that can be computed in terms of far-field quantities. The first method uses information from a small distance away from the crack tip where the stress field is singular and special finite elements are needed for the computation of K_{I} and K_{II}. On the contrary, using far-field quantities is very convenient since it can be carried out within a standard finite element code. In the following, we adopt a procedure based on path-independent integrals J, L, M and $[H]$:

$$J_j(\mathbf{u}^{(1)}) = \int_{S_y} b_{ij}(\mathbf{u}^{(1)})n_i\, ds_y \tag{23}$$

$$L(\mathbf{u}^{(1)}) = \int_{S_y} \varepsilon_{3kj}(y_k b_{ij}(\mathbf{u}^{(1)}) + u_k^{(1)} a_{ijkl} e_{ykl}(\mathbf{u}^{(1)}))n_i\, ds_y \tag{24}$$

$$M(\mathbf{u}^{(1)}) = \int_{S_y} y_j b_{ij}(\mathbf{u}^{(1)})n_i\, ds_y \tag{25}$$

$$[H(\mathbf{u}^{(1)})] = \int_{-d/2}^{+d/2} (W(\mathbf{u}^{(1)})(y'_1,0^+) - W(\mathbf{u}^{(1)})(y'_1,0^-))y'_1\, dy'_1 \tag{26}$$

where ε_{3kj} is the permutation tensor, $\mathrm{b}_{ij}(\mathbf{u}^{(1)})$ is the Eshelby stress tensor:

$$b_{ij}(\mathbf{u}^{(1)}) = \frac{1}{2}a_{mnkl}e_{ykl}(\mathbf{u}^{(1)})e_{ymn}(\mathbf{u}^{(1)})\delta_{ij} - a_{ikmn}e_{ymn}(\mathbf{u}^{(1)})\frac{\partial u_k^{(1)}}{\partial y_j} \tag{27}$$

while y_i, $u_i^{(1)}$ and n_i are the i-component of the position vector, the displacement vector and the unit normal vector computed in the periodic unit cell, respectively. Here y'_i is the abscissa of the coordinate system linked to the crack in the unit cell (Fig. 1). The procedure proposed by Kienzler and Herrmann (2000), described in Appendix, has been followed. It leads to the expression of stress intensity factors with respect to the L-, M- and $[H]$-integrals:

$$K_{\mathrm{I}}(\mathbf{u}^\varepsilon) = \sqrt{\varepsilon}K_{\mathrm{I}}(\mathbf{u}^{(1)}) = \frac{\sqrt{\varepsilon}}{2}\sqrt{\frac{E}{d(1-\nu^2)}} \times \left(\sqrt{M(\mathbf{u}^{(1)}) - (L(\mathbf{u}^{(1)}) - [H(\mathbf{u}^{(1)})])} + \sqrt{M(\mathbf{u}^{(1)}) - (L(\mathbf{u}^{(1)}) + [H(\mathbf{u}^{(1)})])}\right) \tag{28}$$

$$K_{\mathrm{II}}(\mathbf{u}^\varepsilon) = \sqrt{\varepsilon}K_{\mathrm{II}}(\mathbf{u}^{(1)}) = \frac{\sqrt{\varepsilon}}{2}\sqrt{\frac{E}{d(1-\nu^2)}} \times \left(\sqrt{M(\mathbf{u}^{(1)}) - (L(\mathbf{u}^{(1)}) - [H(\mathbf{u}^{(1)})])} - \sqrt{M(\mathbf{u}^{(1)}) - (L(\mathbf{u}^{(1)}) + [H(\mathbf{u}^{(1)})])}\right) \tag{29}$$

These intensity factors are expressed only with $\mathbf{u}^{(1)}$ as a consequence of the fact that, in the asymptotic development, it is only the microscopic displacement $\mathbf{u}^{(1)}$ that is sensitive to the presence of the micro-cracks.

The coefficients K_{I} and K_{II} can be computed for a large number of lengths d and orientations θ of cracks and for the three modes of deformations ($\xi_{\pm}^{11}$, $\xi_{\pm}^{22}$ and $\xi_{\pm}^{12}$) in both states of opening (+) or contact (−) of the crack lips. In this way, we obtain by interpolation the polynomial expressions of $K_{\mathrm{I}}(d,\theta)$ and $K_{\mathrm{II}}(d,\theta)$. In the computations, we used the same material parameters as before. The results of the evolution of stress intensity factors as a function of normalized damage variable $d^\star$ for different orientations θ are presented in Figs. 5 and 6. In the second case, for cracks in contact, K_{I}=0 for any loading mode of the unit cell. The computations have been performed with the finite element code COMSOL AB (2006).

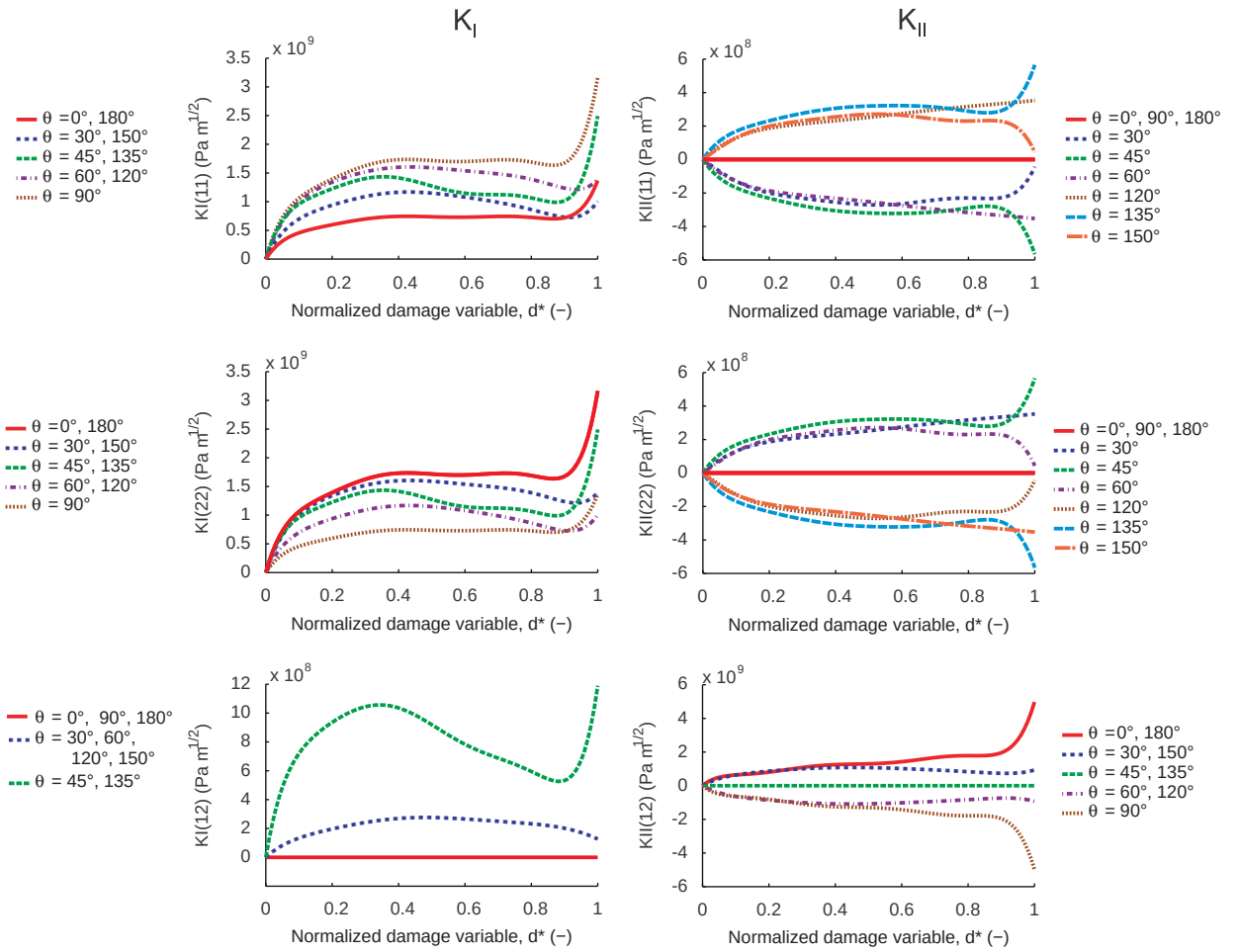

Fig. 5. Evolution of the stress intensity factors K_{I} and K_{II} with respect to the damage variable d and the crack orientation θ for elementary modes of deformation: opening conditions of the crack lips ($\mathbf{R}^{+}$ domain).

In the formulae (28)–(29), the microscopic displacement $\mathbf{u}^{(1)}$ can be expressed with the macroscopic deformation $\mathbf{e}_{\mathbf{x}}(\mathbf{u}^{(0)})$, by using the relation (16). For any macroscopic field $[e_{x11}\ e_{x22}\ e_{x12}]$, the resulting stress intensity factors are determined by the superposition of the stress intensity factors of the elementary deformation modes ($\xi^{11}_{\pm}$, $\xi^{22}_{\pm}$, $\xi^{12}_{\pm}$), as a consequence of (16):

$$K_{\mathrm{I,II}}(\mathbf{u}^{(1)}) = \pm\left(e_{x11}K_{\mathrm{I,II}}(\xi^{11}_{\pm}) + e_{x22}K_{\mathrm{I,II}}(\xi^{22}_{\pm}) + 2e_{x12}K_{\mathrm{I,II}}(\xi^{12}_{\pm})\right) \quad \text{in } \mathbf{R}^{\pm} \tag{30}$$

The distinction between stress intensity factors for opening and closure of micro-cracks is given by the orientation of the force-type vector in the right member of Eq. (12) with respect to crack line (see relation (17)). The stress intensity factors are then obtained by the relations (53) and (54) in the appendix ($K_{\mathrm{I,II}}(\mathbf{u}^{\varepsilon}) = \sqrt{\varepsilon}K_{\mathrm{I,II}}(\mathbf{u}^{(1)})$).

The procedure described previously allows us to compute the stress intensity factors for straight micro-cracks, as functions of the macroscopic deformations. In what follows, we will express the intensity factors for kinks with those for straight cracks and we will replace the kinked cracks by equivalent straight cracks.

3.2. Kinked cracks

In order to apply the subcritical criterion for the growth of micro-crack (Eq. (18)), we consider the direction of crack propagation that maximize the energy release rate. This assumption implies that the crack does not propagate in its own plane but produces a kinking angle as expressed by Eq. (19). Therefore, the mode I stress intensity factor included in the subcritical criterion is not the stress intensity factor of the straight crack K_{I} but $K^{\star}_{\mathrm{I}}$ corresponding to the kinked crack. For short time intervals, the length of the crack propagation dl can be assumed small regarding to the crack length ($dl \ll a$). Under such a condition, the relationship proposed by Leblond (1999) can be used to express $K^{\star}_{\alpha}$ with respect to K_{β}

$$K^{\star}_{\alpha} = F_{\alpha,\beta}(\phi_{max})K_{\beta} \tag{31}$$

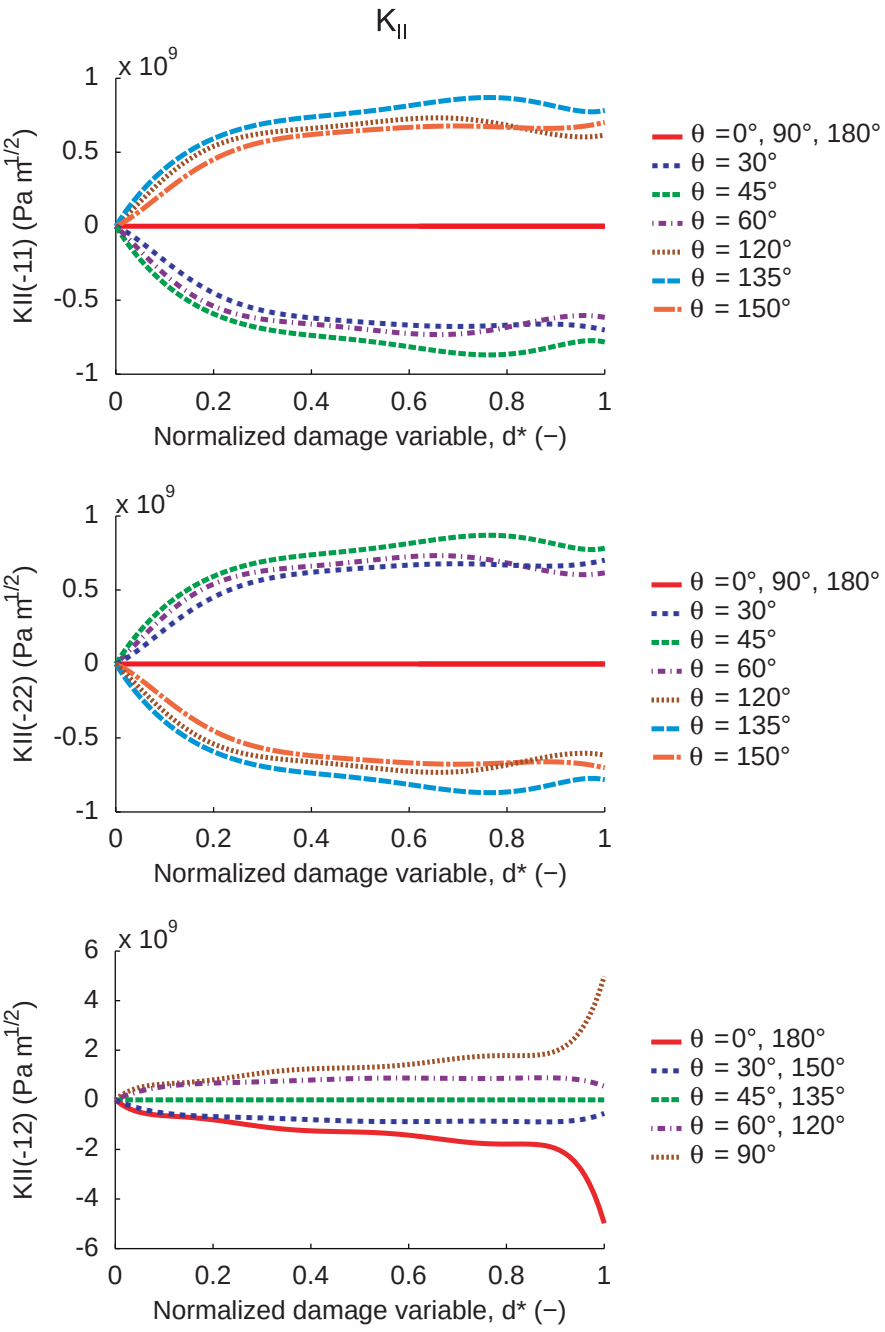

Fig. 6. Evolution of the stress intensity factors K_{II} with respect to the damage variable d and the crack orientation θ for elementary modes of deformation: contact conditions of the crack lips ($\mathbf{R}^-$ domain).

where α and β take the values I and II and $F_{\alpha\beta}(\phi_{max})$ is a 2×2 matrix depending on the kinking angle ϕ_{max}. The main advantage of this expression is that it is universal, with respect to the geometry and the loading. The geometric and mechanical parameters are directly included in K_β. The analytical expression of the functions $F_{I,I}$, $F_{I,II}$, $F_{II,I}$ and $F_{II,II}$ are given with respect to the kinking angle through polynomials of order 20 by Leblond (1999).

Many authors (e.g. Nemat-Nasser and Horii, 1982) have shown that the determination of the kinking angle through the maximum energy release rate gives essentially the same results than the condition of local symmetry which requires that the mode II stress intensity factor vanishes at the tip of the kinked extension. Therefore, we can neglect the mode II intensity factor ($K_{II}^\star = 0$).

4. Equivalent crack

The determination of the direction (ϕ_{max}, Eq. (19)) and the length (dl, Eq. (18)) of the out-of-plane crack extension is not enough to compute the whole trajectory of the crack tips. Indeed, after the first increments of computation, the initial straight crack may kink. At this stage, the above theory using the K_α of the smooth crack is no more valid because the obtained crack is now a kinked crack and the subsequent crack extension would start from that kinked crack. There are several possible ways to replace the kinked crack by an equivalent straight crack. For instance, Schütte and Bruhns (2002) proposed to find, at each time step, a straight crack that is thermodynamically equivalent to the kinked crack. Baud and Reuschlé (1997) introduce an equivalent straight crack by joining the tips of the real branched crack. In this paper, we adopt this last solution for the construction of the equivalent crack, which is obtained by joining the tips of the real branched crack (Fig. 7).

The equivalent crack is determined after each step of calculation by means of geometrical relationships, as follows for the crack orientation:

$$\tan(d\theta) = \frac{\sin(\phi_{max})}{\frac{a_n}{dl} + \cos(\phi_{max})} \tag{32}$$

and for the updated crack length:

$$a_{n+1} = \frac{\sin(\phi_{max})}{\sin(d\theta)}\, dl \tag{33}$$

where a_n and a_{n+1} are the length of the straight crack at steps n and $n+1$ (Fig. 7).

Assuming small time increments, equating $d\theta \simeq \tan(d\theta) \simeq \sin(d\theta)$ that result from Eqs. (32) and (33) and using the up-scaling relation (1), the two last expressions can be transformed, at the limit, into differential equations:

$$\frac{dd}{dt} = \frac{2}{\varepsilon}\cos(\phi_{max})\frac{dl}{dt} \tag{34}$$

$$\frac{d\theta}{dt} = \frac{2}{\varepsilon d}\sin(\phi_{max})\frac{dl}{dt} \tag{35}$$

These last two equations show that the geometry of the equivalent micro-crack, in terms of length and orientation, depends on the propagation rate dl/dt and the orientation ϕ_{max} of the kinked crack. These quantities are computed with respect to the stress intensity factor K_I and K_{II} of the equivalent straight micro-cracks, as shown previously. They depend on the macroscopic damage variables d and θ and on the macroscopic deformation $\mathbf{e_x}$. This establishes the homogenized damage model, based on mixed micro-crack propagation, in an implicit form. We remark the presence of the micro-structural length parameter ε in the damage equations (34) and (35).

5. Numerical examples

5.1. Computation algorithm

In order to study the local macroscopic response, we analyze the problem by the governing equations (18) and (19) at crack tip level, the differential equations (34) and (35) linking the micro-crack level to the macroscopic one and the homogenized law (14) at macroscopic level. The input of this system of equations will be the macroscopic stress or strain, depending on the physical problem to be studied.

Due to the dependency of the macroscopic elastic modulus C_{ijkl} on the damage variable d and on the crack orientation θ, and due to the non-linear evolution of the stress intensity factors with the state of strain, the problem is highly non-linear. For each time step, the problem is solved by an iterative procedure as follows:

1. Initialization ($n=1$):
   $d_0^t = d^{t-1}$ and $\theta_0^t = \theta^{t-1}$ (if $t=0$, $d_0 = d^0$ and $\theta_0 = \theta^0$).

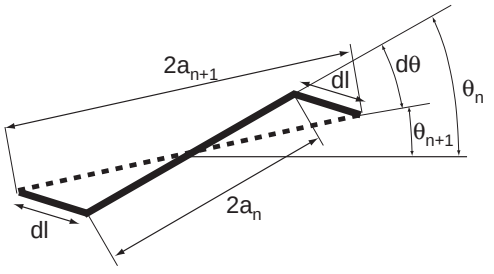

Fig. 7. The kinked crack (solid line) with its equivalent replacement crack (dashed line). In this figure, the crack rotation $d\theta$ is negative.

2. Determination of the homogenized coefficient:
   $C_{ijkl} = C_{ijkl}(d^t_{n-1}, \theta^t_{n-1})$.
3. Prediction of the macroscopic strain:
   $e_{xij,n-1} = C^{-1}_{ijkl}(d^t_{n-1}, \theta^t_{n-1})\Sigma^{(0)}_{ij}$.
4. Determination of the stress intensity factors:
   $K_{I,II} = K_{I,II}(C_{ijkl}(d^t_{n-1}, \theta^t_{n-1}))$;
   $K^{\star}_{I,II} = K^{\star}_{I,II}(K_{I,II})$.
5. Computation of the propagation rate:
   $dl/dt = dl/dt(K^{\star}_{I,II})$.
6. Update of the damage variables:
   $dd/dt = dd/dt(dl,\varepsilon)$; $d^t_n = d^{t-1} + \Delta t dd/dt$;
   $d\theta/dt = d\theta/dt(d,dl,\varepsilon)$; $\theta^t_n = \theta^{t-1} + \Delta t d\theta/dt$.
7. Update of the homogenized coefficient:
   $C_{ijkl} = C_{ijkl}(d^t_n, \theta^t_n)$.
8. Calculation of the updated strain:
   $e_{xij,n} = C^{-1}_{ijkl}(d^t_n)\Sigma^{(0)}_{ij}$.
9. Convergence of the solution is tested:
   $CONV = \|\mathbf{e}_n - \mathbf{e}_{n-1}\|^2 / \|\mathbf{e}_n\|^2$.
   (i) If $CONV \leq Tol$: Return to point 1 with a new time step (t=t+1).
   (ii) If $CONV > Tol$: Return to point 2 with n=n+1,

where n is the iteration step, t is the time step number, Δt is the size of the time step, d^0 and θ^0 are the initial damage and initial orientation of the micro-cracks and Tol is the tolerance taken as 10^{-5}.

We note that, because the homogenized coefficients (15) and the stress intensity factors (28)–(29) are written in terms of macroscopic strain, this procedure becomes trivial in the strain control case.

5.2. Numerical simulations

The time-dependent behavior of materials can be underlined by means of various laboratory tests. In particular, quasi-static loading tests, creep tests or relaxation tests may point out the same time-dependent properties under different stress and strain conditions. The response of materials observed during quasi-static compression tests is generally affected by the axial strain rate $\dot{\boldsymbol{e}}_{\mathbf{x}}$. Higher is the strain rate (i.e. faster is the loading) and higher is the strength. When $\dot{e}_x$ is sufficiently low, the micro-cracking has enough time to develop inducing a decrease of the material strength. Under the condition of creep tests (i.e. keeping a constant stress level), the failure is no more governed by the maximal stress that the material may sustain but rather by the time needed for the micro-cracks to propagate under subcritical conditions. Also, upon a relaxation test, obtained by keeping a constant strain level, the micro-crack may propagate until failure of the material, even if the loading is not evolving in time. The higher the strain level, the faster the failure.

The set of material parameters that have been used in the simulations are reported in Table 1. All the simulations presented in the following have been made considering biaxial loading. According to the considered tests, the loading is stress- and/or strain-controlled in the vertical and horizontal directions. Plane-strain condition is considered in the third direction.

5.2.1. Loading at constant strain rate

Figs. 8–10 illustrate the response of a material defined by the parameters reported in Table 1 submitted to uniaxial tension loading. A constant vertical strain rate is imposed and the horizontal direction is free of stress. Fig. 8 shows that the developed model is able to reproduce the effect of strain rate on the obtained failure stress. Under low strain rate, the effect of time becomes predominant and the failure appears for a lower strain level than in the case of faster loading.

At the onset of loading, under weak strain level, the stress intensity factors in mode I at the crack tips ($K^{\star}_I$) are low. As a consequence, the subcritical strain rate, which is computed with respect to $K^{\star}_I$ (Eq. (18)), is low and the damage variable d and the orientation of the crack θ remain almost constant (Fig. 9). As a consequence, the rigidity of the material is not modified during the first part of the loading and the behavior is more or less linear. Then, when the strain level becomes sufficiently high, the combined effect of high $K^{\star}_I$ and time makes that the damage increases in the material. However, the micro-cracks are not growing in their own plane but a kinked angle is forming in order to propagate in the direction that

Table 1
Material parameters used in the simulations.

E (Pa)	ν (–)	K_0 (MPa m$^{1/2}$)	v_0 (m/s)	n (–)	ε (–)	d^0 (–)	θ^0 (deg)
2×10^9	0.3	0.6	1×10^{-3}	20	1×10^{-4}	0.28	45

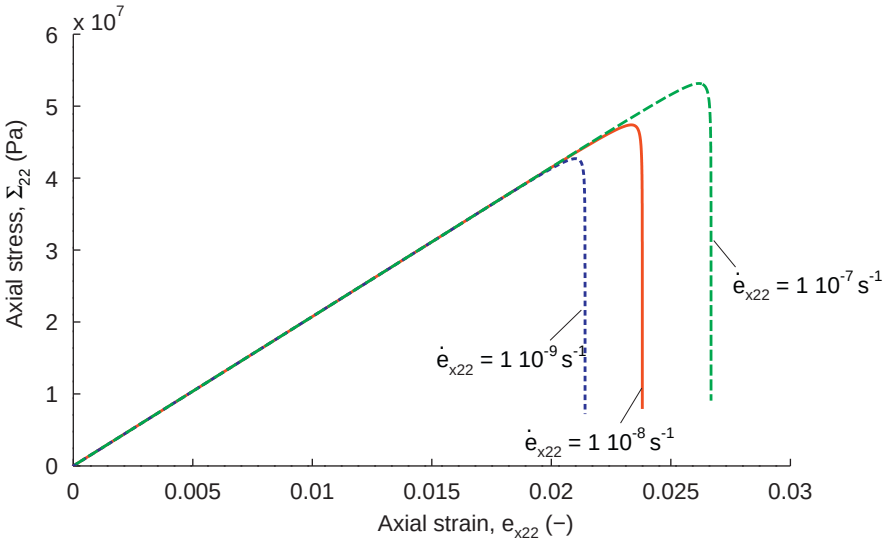

Fig. 8. Axial tension tests at various constant strain rate $\dot{e}_{x22}$. The strength increases when the strain rate increases.

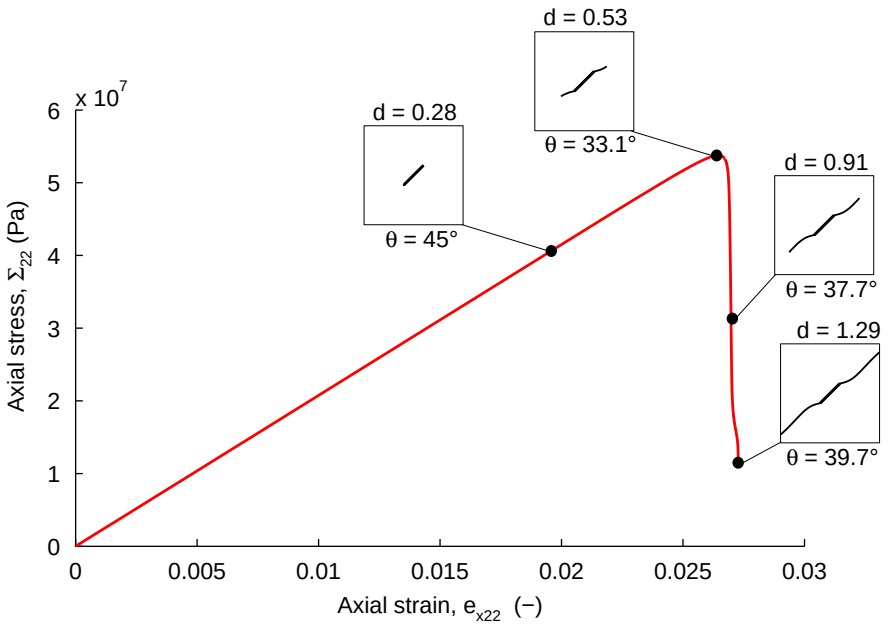

Fig. 9. Axial tension test at a constant strain rate $\dot{e}_{x22} = 1 \times 10^{-8}\ s^{-1}$. Evolution of the micro-crack in the periodic cell.

maximizes the energy release rate (Eq. (19)). As the damage increases, the equivalent crack is rotating and the rigidity decreases until coalescence of micro-cracks producing failure of the material. At the end of the loading, the equivalent cracks tend to be perpendicular to the direction of the principal tensile strain. Because of the anisotropic response of the material induced by the oriented crack, the periodic cells are subject to a shearing that induce a rotation of the principal strain with respect to the principal stress. This explains that the final equivalent crack is not perpendicular to the applied tensile stress (Fig. 9).

Fig. 10 shows the effect of two main parameters, the subcritical exponent and the micro-structural length, on the response of the material under a tension test at constant strain rate. When the stress intensity factor $K_I^\star$ is lower than the referential stress intensity factor K_0, the fraction of Eq. (18) is less than unity. In that case, an increase of the subcritical exponent decreases the rate of crack propagation and postpones the failure of the material, as observed in Fig. 10a. For a same loading level, K_I and K_{II} increase with the internal length ε (Eqs. (28)–(29)), inducing a faster failure of the structure (Fig. 10b). In other words, the finer is the micro-structure, the more resistant is the material.

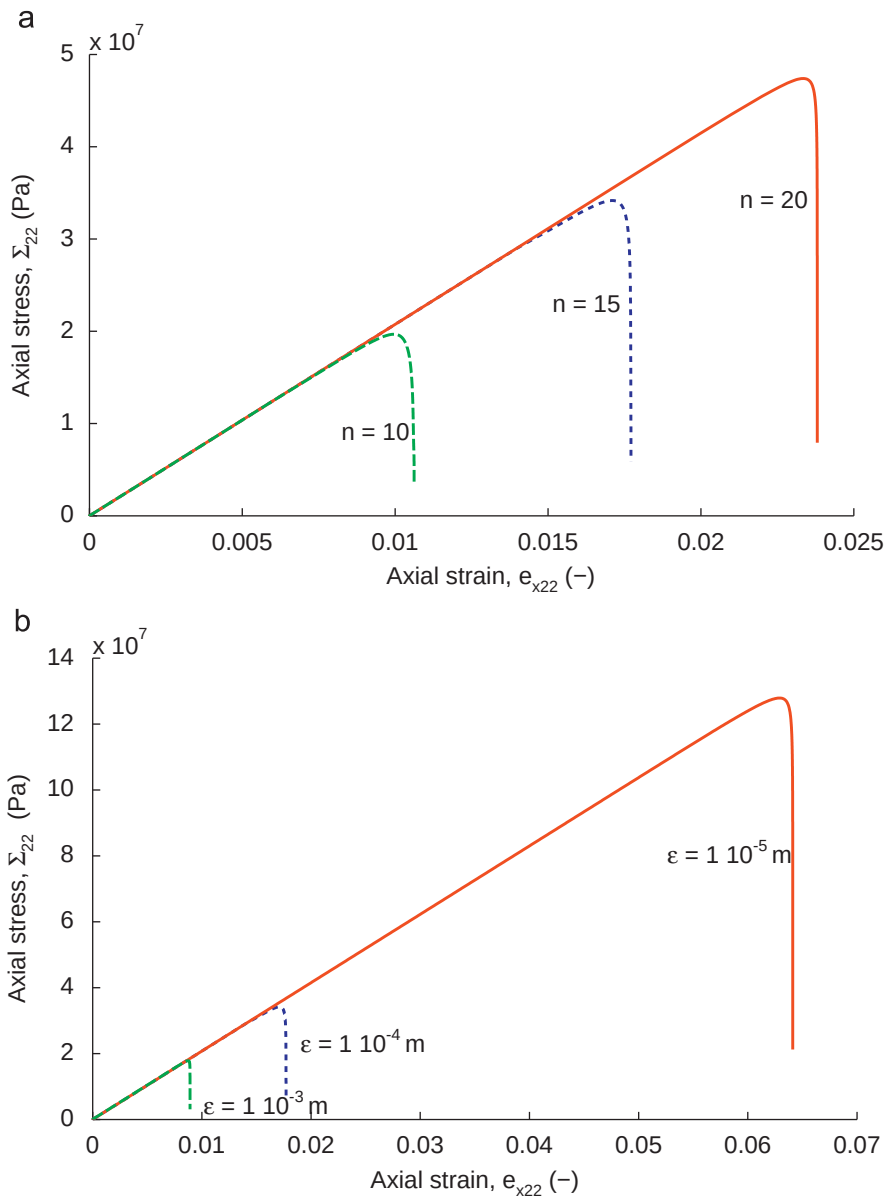

Fig. 10. Axial tension test at a constant strain rate $\dot{e}_{x22} = 1 \times 10^{-8}\ s^{-1}$. Effect of the variation of the subcritical exponent (a) and of the internal length (b).

Fig. 11 shows the evolution of vertical stress with respect to the applied vertical strain along a biaxial test at constant strain rate. The vertical and horizontal strains are both in tension. A constant ratio between both strains is kept all along the test. e_{x11} induces a rotation of the equivalent crack toward the vertical direction while e_{x22} would tend to orient it toward the horizontal one. e_{x22} being higher than e_{x11}, the crack rotates toward horizontal. An increasing horizontal tensile strain with respect to the vertical tensile strain induces an acceleration of the failure and a decrease of the amount of crack rotation. When $e_{x11}=0$ the amount of crack rotation is maximum (cell number 4) while equality between e_{x11} and e_{x22} induces that the micro-crack propagates without rotation. The initial crack being oriented at 45° with respect to both strains, $e_{x11}=e_{x22}$ produces a symmetric strain state with respect to the crack. K_{II} is equal to zero that makes that no rotation is possible.

Fig. 12 shows the evolution of vertical stress with respect to the applied vertical strain along a compressive biaxial test at constant strain rate. The vertical and horizontal strains are both in compression. A constant ratio between both strains is kept all along the test. Contrary to tension tests, the compression tests produces a propagation of the crack tending asymptotically to a given crack length and crack orientation, without reaching coalescence of micro-cracks. The micro-cracks grow and rotate until reaching a situation for which $K_I=K_{II}=0$. Under such a configuration, no more propagation is possible. The length and the orientation of the crack that produce such an equilibrium case depends on the initial situation

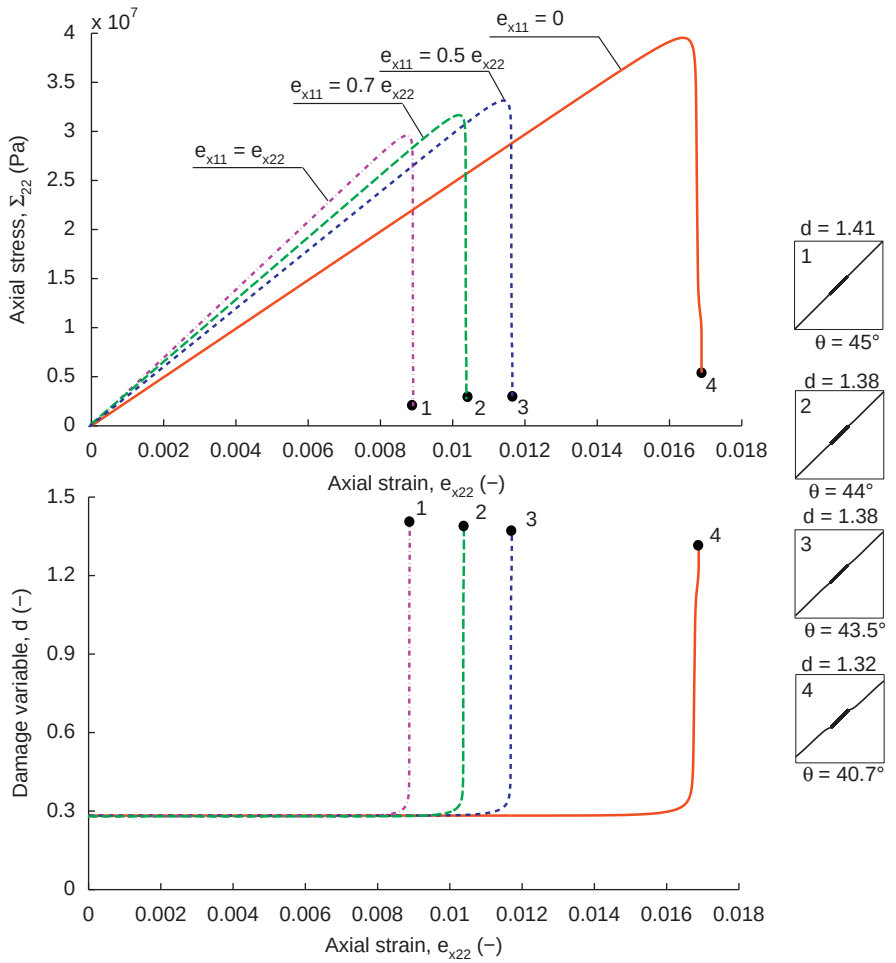

Fig. 11. Biaxial test at constant strain rate ($\dot{e}_{x22} = 1 \times 10^{-8}\ s^{-1}$), e_{x22} and e_{x11} in tension with a constant ratio between both strain ($e_{x22} \geq e_{x11}$).

and the loading conditions (i.e. the ratio between both strains, in our case). Closer to one is the ratio between e_{x11} and e_{x22} lower is the amount of crack rotation. In the limit case, when $e_{x11}=e_{x22}$, the initial crack being oriented at 45° with respect to both loading directions, $K_I=K_{II}=0$ under the initial configuration and the micro-cracks do not propagate. Contrary to the tension test, the damage increase does not induce degradation of the material rigidity. Under contact conditions of the crack lips, the drop of homogenized coefficient C_{1111} and C_{2222} are compensated by an enhancement of C_{1122} by the same amount (Fig. 3). Consequently, the ratio between Σ_{22} and e_{x22} is not affected by the damage increase (i.e. the slope of the curve remain constant), even if the damage variable increases all along the compression test. So, looking only the stress evolution, it could seem that axial compression does not damage material. However, the micro-cracks has propagated and a subsequent change in the loading direction (a tensile loading, for instance) would induce a faster failure than in the case without the preliminary compression phase.

5.2.2. *Relaxation tests*

Applying a constant axial strain, the relaxation test aims at investigating the time-dependent response of material. Under a constant loading, the subcritical micro-crack growth produces a progressive decrease of the rigidity as long as the damage state increases. As a consequence, the stresses are gradually relaxing upon failure. Under a biaxial combined tensile/compressive constant strain field ($e_{x22}=-0.035$ (compression) and $e_{x11}=0.035$ (tension)), Fig. 13 shows the evolution of horizontal and vertical stresses with time. In parallel, the evolution with time of the ratio between horizontal and vertical stress is shown. The non-planar growth of micro-cracks produces a rotation of the equivalent cracks to be oriented perpendicularly to the principal tensile strain, that is parallel to the principal compressive strain. As long as the crack propagate, the direction of the equivalent crack tends toward vertical. As a consequence, the crack lips being under opening condition, the horizontal rigidity becomes much lower than vertical one. So, the ratio between horizontal and vertical stresses evolves in accordance with the relative lost of horizontal rigidity with respect to vertical one. That is a characteristic of the evolving anisotropic damage law.

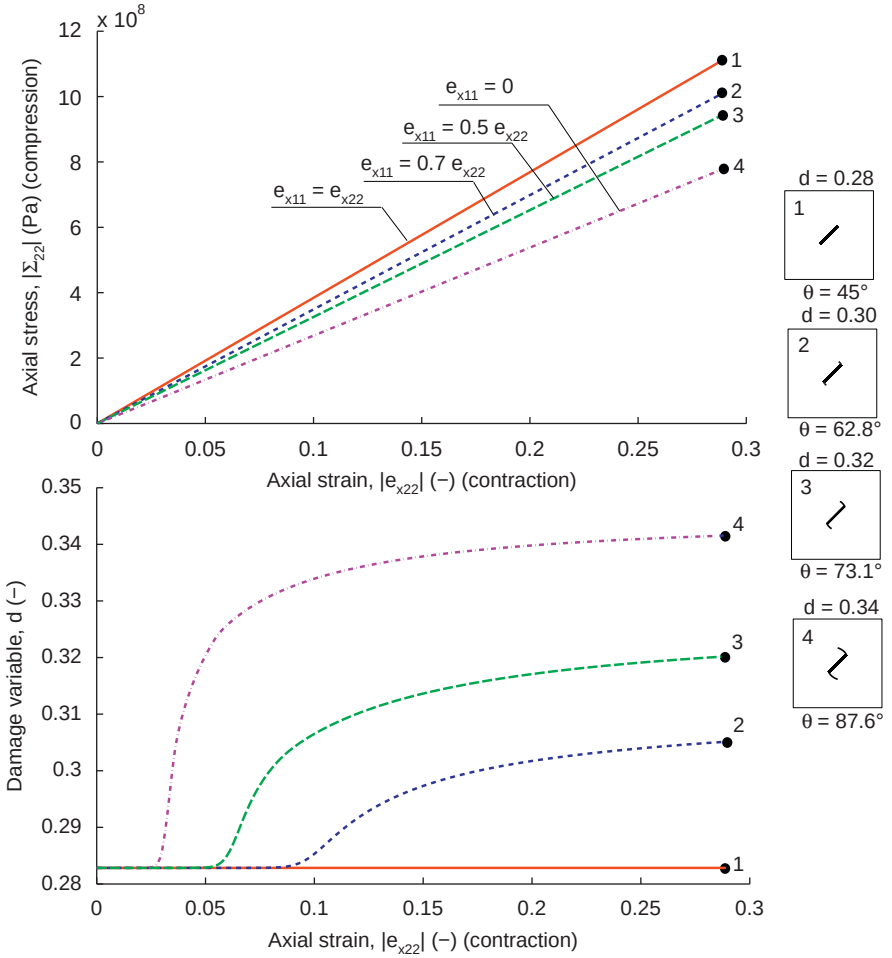

Fig. 12. Biaxial test at constant strain rate ($\dot{e}_{x22} = 1 \times 10^{-8}\,\mathrm{s}^{-1}$), e_{x22} and e_{x11} in compression with a constant ratio between both strain and $|e_{x22}| \geq |e_{x11}|$.

5.2.3. *Creep tests*

Fig. 14 depicts the creep strain predicted by the model under a biaxial combined tensile/compressive constant stress field ($\Sigma_{22} = -50\,\mathrm{MPa}$ (compression) and $\Sigma_{11} = 50\,\mathrm{MPa}$ (tension)). After an instantaneous strain response corresponding to the short-term behavior of the material, the time effect makes damage variable increase and micro-cracks rotate. During the first part of the test, the damage evolution is slow. However, the rate of damage is amplifying with time. Indeed, under constant stress field, as long as the damage increases, the strain field increases which enhances the stress intensity factor at the crack tips. Consequently, the higher the damage, the higher the strain and the higher the rate of propagation of micro-cracks. The same comments as for the relaxation case can be done about the anisotropic response of the material.

6. Conclusions

A subcritical two-scale damage model based on kinking of micro-cracks has been deduced. A locally periodic micro-structure has been assumed and homogenization based on asymptotic developments has been used to deduce the macroscopic elasto-damage model. A subcritical propagation criterion has been employed to describe the evolution of kinked micro-cracks. The direction of propagation has been given by the maximum energy release criterion.

In order to consider arbitrary orientations of micro-cracks in an efficient two-scale approach, the kinked crack obtained at each step of calculation has been replaced by an equivalent straight crack defined by its length and its orientation. Two regimes, corresponding to open or closed micro-cracks, are considered, leading to different effective damage behaviors in tension or compression.

As long as the micro-cracks grow due to the combined effect of time and high stresses at the crack tips, the internal damage increases and the global rigidity of the material decreases. That has been quantified by means of a series of finite element simulations on a unit cell. Databases of effective elastic coefficients and stress intensity factors in modes I and II,

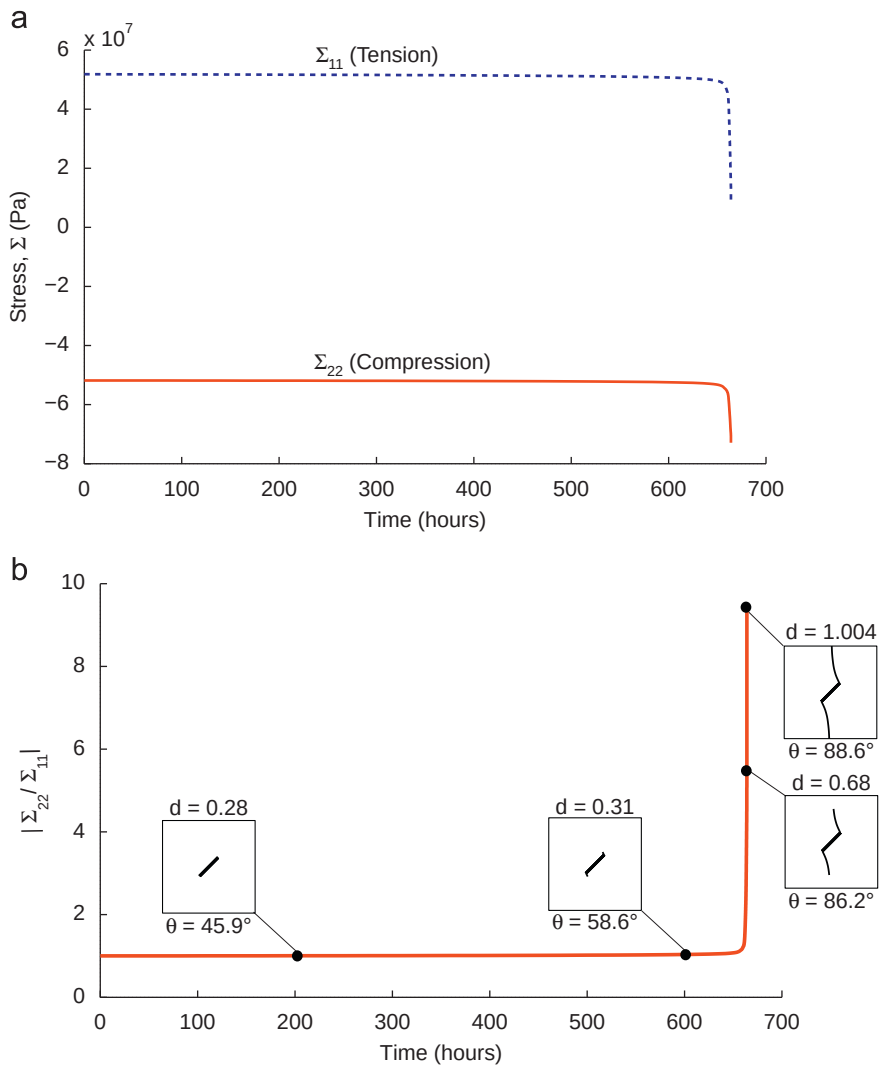

Fig. 13. Relaxation test under biaxial conditions. $e_{x22} = -0.035$ (compression) and $e_{x11} = 0.035$ (tension). Evolution with time of the horizontal and vertical stresses (a) and of the ratio of anisotropy, defined as the absolute value of the stress ratio (b).

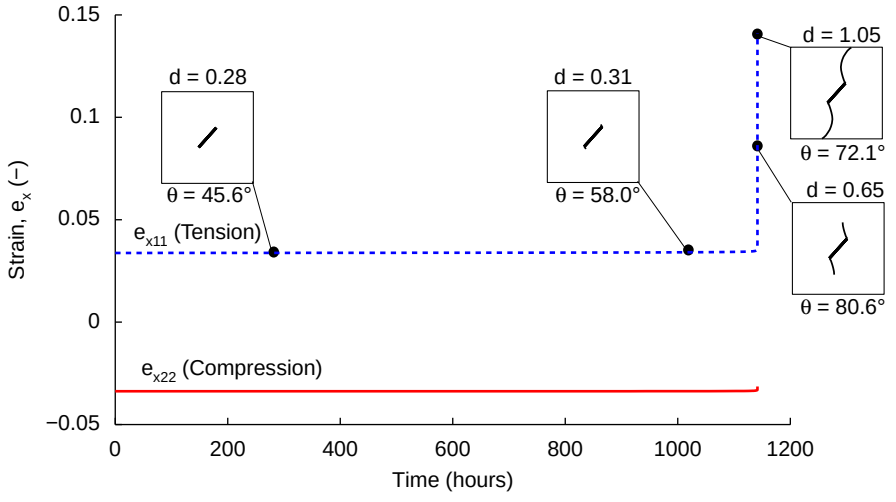

Fig. 14. Creep test under biaxial conditions. $\Sigma_{22} = -50$ MPa (compression) and $\Sigma_{11} = 50$ MPa (tension). Evolution of the horizontal and vertical strain with time.

obtained for elementary modes of deformation of the unit cell are *a priori* computed for different orientations and lengths of micro-cracks, in opening and closure regimes. A procedure based on path-independent integrals has been used for the computation of the stress intensity factors. These stress intensity factors are directly used to quantify the rate and the orientation of the out-of-plane subcritical crack growth.

The time-dependent macroscopic damage model has been deduced and the effective stress–strain and damage responses, depending on time, have been numerically evaluated in a macroscopic point. Numerical simulations of loading at constant strain rate, relaxation or creep tests, under tension or compression, have shown the ability of the developed model to reproduce known time-dependent damage responses.

Acknowledgements

This work was funded by the French National Agency for Radioactive Waste Management (ANDRA). The authors wish to acknowledge the financial support.

Appendix

The procedure to determine the stress intensity factors for a straight micro-crack trajectory uses the *J*-, *L*- and *M*-integrals (Kienzler and Herrmann, 2000), computed in the unit periodic cell:

$$J_j(\mathbf{u}^{(1)}) = \int_{S_y} b_{ij}(\mathbf{u}^{(1)}) n_i \, ds_y \tag{36}$$

$$L(\mathbf{u}^{(1)}) = \int_{S_y} \varepsilon_{3kj}(y_k b_{ij}(\mathbf{u}^{(1)}) + u_k^{(1)} a_{ijkl} e_{ykl}(\mathbf{u}^{(1)})) n_i \, ds_y \tag{37}$$

$$M(\mathbf{u}^{(1)}) = \int_{S_y} y_j b_{ij}(\mathbf{u}^{(1)}) n_i \, ds_y \tag{38}$$

where ε_{3kj} is the permutation tensor

$$\varepsilon_{ijk} = \begin{cases} 1 & \text{if } ijk = 123,231,312 \\ -1 & \text{if } ijk = 132,321,213 \\ 0 & \text{otherwise} \end{cases} \tag{39}$$

and b_{ij} is the Eshelby stress tensor

$$b_{ij}(\mathbf{u}^{(1)}) = \frac{1}{2} a_{mnkl} e_{ykl}(\mathbf{u}^{(1)}) e_{ymn}(\mathbf{u}^{(1)}) \delta_{ij} - a_{ikmn} e_{ymn}(\mathbf{u}^{(1)}) \frac{\partial u_k^{(1)}}{\partial y_j} \tag{40}$$

y_i, $u_i^{(1)}$ and n_i are the i-component of the position vector, the displacement vector and the unit normal vector computed in the unit cell, respectively.

For crack faces free of applied tension or with frictionless contact, the following result is obtained:

$$J_1(\mathbf{u}^{(1)}) = J_1^r(\mathbf{u}^{(1)}) + J_1^l(\mathbf{u}^{(1)}) \tag{41}$$

$$J_2(\mathbf{u}^{(1)}) = J_2^r(\mathbf{u}^{(1)}) + J_2^l(\mathbf{u}^{(1)}) + [W(\mathbf{u}^{(1)})] \tag{42}$$

$$L(\mathbf{u}^{(1)}) = \frac{d}{2}(J_2^r(\mathbf{u}^{(1)}) - J_2^l(\mathbf{u}^{(1)})) + [H(\mathbf{u}^{(1)})] \tag{43}$$

$$M(\mathbf{u}^{(1)}) = \frac{d}{2}(J_1^r(\mathbf{u}^{(1)}) - J_1^l(\mathbf{u}^{(1)})) \tag{44}$$

where $J_i^r(\mathbf{u}^{(1)})$ and $J_i^l(\mathbf{u}^{(1)})$ are Rice's *J*-integrals around the right and left crack tips computed in the unit cell, respectively, and $[W(\mathbf{u}^{(1)})]$ and $[H(\mathbf{u}^{(1)})]$ are the jump across the crack of the integral on the crack faces of $W(\mathbf{u}^{(1)}) = \frac{1}{2} a_{mnkl} e_{ykl}(\mathbf{u}^{(1)}) e_{mn}$ and $H(\mathbf{u}^{(1)}) = y'_1 W(\mathbf{u}^{(1)})$, respectively:

$$[W(\mathbf{u}^{(1)})] = \int_{-d/2}^{+d/2} (W(\mathbf{u}^{(1)})(y'_1, 0^+) - W(\mathbf{u}^{(1)})(y'_1, 0^-)) \, dy'_1 \tag{45}$$

$$[H(\mathbf{u}^{(1)})] = \int_{-d/2}^{+d/2} (W(\mathbf{u}^{(1)})(y'_1, 0^+) - W(\mathbf{u}^{(1)})(y'_1, 0^-)) y'_1 \, dy'_1 \tag{46}$$

where y'_1 is the abscissa of the coordinate system linked to the crack in the unit cell.

The considered cracks being symmetric, we have $J_i^r(\mathbf{u}^{(1)}) = -J_i^l(\mathbf{u}^{(1)})$ and $[W(\mathbf{u}^{(1)})]=0$. Through Eqs. (41) and (42), it makes that $J_1(\mathbf{u}^{(1)}) = -J_2(\mathbf{u}^{(1)}) = 0$. From Eqs. (43) and (44), we obtain

$$J_1^r(\mathbf{u}^{(1)}) = -J_1^l(\mathbf{u}^{(1)}) = \frac{M(\mathbf{u}^{(1)})}{d} \tag{47}$$

$$J_2^r(\mathbf{u}^{(1)}) = -J_2^l(\mathbf{u}^{(1)}) = \frac{L(\mathbf{u}^{(1)})-[H(\mathbf{u}^{(1)})]}{d} \tag{48}$$

Those two Rice's J-integrals may be expressed with respect to the stress intensity factors in modes I and II, by the well-known expressions:

$$J_1^r(\mathbf{u}^{(1)}) = \frac{1-\nu^2}{E}[K_{\mathrm{I}}(\mathbf{u}^{(1)})^2 + K_{\mathrm{II}}(\mathbf{u}^{(1)})^2] \tag{49}$$

$$J_2^r(\mathbf{u}^{(1)}) = -2\frac{1-\nu^2}{E}K_{\mathrm{I}}(\mathbf{u}^{(1)})K_{\mathrm{II}}(\mathbf{u}^{(1)}) \tag{50}$$

Combination of Eqs. (47)–(50) yields to the expression of stress intensity factors with respect to the L-, M- and $[H]$-integrals:

$$K_{\mathrm{I}}(\mathbf{u}^{(1)}) = \frac{1}{2}\sqrt{\frac{E}{d(1-\nu^2)}} \times \left(\sqrt{M(\mathbf{u}^{(1)})-(L(\mathbf{u}^{(1)})-[H(\mathbf{u}^{(1)})])} + \sqrt{M(\mathbf{u}^{(1)})-(L(\mathbf{u}^{(1)})+[H(\mathbf{u}^{(1)})])}\right) \tag{51}$$

$$K_{\mathrm{II}}(\mathbf{u}^{(1)}) = \frac{1}{2}\sqrt{\frac{E}{d(1-\nu^2)}} \times \left(\sqrt{M(\mathbf{u}^{(1)})-(L(\mathbf{u}^{(1)})-[H(\mathbf{u}^{(1)})])} - \sqrt{M(\mathbf{u}^{(1)})-(L(\mathbf{u}^{(1)})+[H(\mathbf{u}^{(1)})])}\right) \tag{52}$$

The upscaling procedure ($d = 2a/\varepsilon$, $\mathbf{y} = \mathbf{x}/\varepsilon$ and $\mathbf{y}' = \mathbf{x}'/\varepsilon$, $ds_y = dS/\varepsilon$ and $\mathbf{u}^{\varepsilon} \simeq \mathbf{u}^{(0)}(\mathbf{x}) + \varepsilon\mathbf{u}^{(1)}(\mathbf{x},\mathbf{y})$, $\mathbf{u}^{(0)}$ being independent of the microscopic variable $\mathbf{y}$) enables us to express K_{I} and K_{II} in the macroscopic problem:

$$K_{\mathrm{I}}(\mathbf{u}^{\varepsilon}) = \sqrt{\varepsilon}K_{\mathrm{I}}(\mathbf{u}^{(1)}) \tag{53}$$

$$K_{\mathrm{II}}(\mathbf{u}^{\varepsilon}) = \sqrt{\varepsilon}K_{\mathrm{II}}(\mathbf{u}^{(1)}) \tag{54}$$

References

Anderson, O., Grew, P., 1977. Stress corrosion theory of crack propagation with applications to geophysics. Reviews of Geophysics and Space Physics 15, 77–104.

Andrieux, S., Bamberger, Y., Marigo, J.J., 1986. Un modèle de matériau microfissuré pour les roches et les bétons. Journal de Mécanique Théorique et Appliquée 5, 471–513.

Atkinson, B., Meredith, P., 1987. The theory of subcritical crack growth with applications to minerals and rocks. In: Fracture Mechanics of Rocks. Academic Press Inc., pp. 111–166.

Bhattacharya, K., Ortiz, M., Ravichandran, G., 1998. Energy-based model of compression splitting in heterogeneous brittle solids. J. Mech. Phys. Solids 46, 2171–2181.

Baud, P., Reuschlé, T., 1997. A theoretical approach to the propagation of interacting cracks. Geophys. J. Int. 130, 460–468.

Benssousan, A., Lions, J., Papanicolaou, G., 1978. Asymptotic Analysis for Periodic Structures. Kluwer Academic Publisher, Amsterdam.

Carol, I., Rizzi, E., Willam, K., 2001. On the formulation of anisotropic elastic degradation. I: theory based on a pseudo-logarithmic damage tensor rate. Int. J. Solid Struct. 38, 491–518.

Chaboche, J.L., 1992. Damage induced anisotropy: on the difficulties associated with the active/passive unilateral condition. Int. J. Damage Mech. 1, 148–171.

Charles, R., 1958. Dynamic fatigue of glass. J. Appl. Phys. 29, 1657–1662.

COMSOL AB, 2006. COMSOL Multiphysics Users Guide. Version 3.3 Documentation.

Dascalu, C., Bilbie, G., 2007. A multiscale approach to damage configurational forces. Int. J. Fract. 147, 285–293.

Dascalu, C., Bilbie, G., Agiasofitou, E., 2008. Damage and size effect in elastic solids: a homogenization approach. Int. J. Solid Struct. 45, 409–430.

Dascalu, C., 2009. A two-scale damage model with material length. C.R. Mec. 337, 645–652.

Dascalu, C., François, B., Keita, O., 2010. A two-scale model for subcritical damage propagation. Int. J. Solid Struct. 47, 493–502.

Dartois, S., Nadot-Martin, C., Halm, D., Dragon, A., Fanget, A., 2009. Discrete damage modelling of highly-filled composites via a direct multiscale "morphological approach". J. Multiscale Modelling 1, 347–368.

Dong, C.Y., Lee, K.Y., 2005. Numerical analysis of doubly periodic array of cracks/rigid-line inclusions in an infinite isotropic medium using boundary integral equation method. Int. J. Fract. 133, 389–405.

Dragon, A., Mroz, Z., 1979. A continuum model for plastic-brittle behaviour of rock and concrete. Int. J. Eng. Sci. 17, 121–137.

Griffith, A., 1921. The phenomena of rupture and flow in solids. Philos. Trans. Royal Soc. London A 221, 163–198.

Horii, H., Nemat-Nasser, S., 1985. Compression-induced microcrack growth in brittle solids: axial splitting and shear. J. Geophys. Res. 90, 3105–3125.

Hu, K.X., Chandra, A., 1993. Interactions among general systems of cracks and anticracks: an integral equation approach. J. Appl. Mech. 60, 920–928.

Huang, C., Subhash, G., 2003. Influence of lateral confinement on dynamic damage evolution during axial compressive response of brittle solids. J. Mech. Phys. Solids 51, 1089–1105.

Kachanov, M., 2007. On the effective elastic properties of cracked solids. Int. J. Fract. 146, 295–299.

Karihaloo, B.L., Wang, J., 1997. On the solution of doubly array of cracks. Mech. Mater. 26, 205–212.

Kemeny, J., 2005. Time-dependent drift degradation due to the progressive failure of rock bridges along discontinuities. Int. J. Rock Mech. Min. Sci. 42, 35–46.

Kienzler, R., Herrmann, G., 2000. Mechanics in Material Space with Applications to Defect and Fracture Mechanics. Springer-Verlag, Berlin, Heidelberg.

Lauterbach, J.B., Gross, D., 1998. Crack growth in brittle solids under compression. Mech. Mater. 29, 81–92.

Leblond, J.B., 1999. Crack paths in three-dimensional elastic solids. I: two-term expansion of the stress intensity factors—application to crack path stability in hydraulic fracturing. Int. J. Solids Struct. 36, 79–103.

Leguillon, D., Sanchez-Palencia, E., 1982. On the behavior of a cracked elastic body with (or without) friction. J. Mech. Theor. Appl. 1, 195–209.
Lene, F., 1986. Damage constitutive relations for composite materials. Eng. Fract. Mech. 25, 713–728.
Liu, W.K., Chen, Y.J., Belytschko, T., Lua, Y.J., 1996. Three reliability methods for fatigue crack growth. Eng. Fract. Mech. 53, 733–752.
Lua, Y.J., Liu, W.K., Belytschko, T., 1992a. A stochastic damage model for the rupture prediction of a multi-phase solid. Part I: parametric studies. Int. J. Fract. 53, 321–340.
Lua, Y.J., Liu, W.K., Belytschko, T., 1992b. A stochastic damage model for the rupture prediction of a multi-phase solid. Part II: statistical approach. Int. J. Fract. 53, 341–361.
Main, I., 2000. A damage mechanics model for power-law creep and earthquake aftershock and foreshock sequences. Geophys. J. Int. 142, 151–161.
Miura, K., Okui, Y., Horii, H., 2003. Micromechanics-based prediction of creep failure of hardrock for long-term safety of high-level radioactive waste disposal system. Mech. Mater. 35, 587–601.
Murakami, Y., Aoki, S., 1987. Stress Intensity Factors Handbook. Pergamon, Oxford, New York.
Muskhelishvili, N.I., 1953. Some Basic Problem of the Mathematical Theory of Elasticity. Noordhoff, The Netherlands.
Nemat-Nasser, S., Horii, H., 1982. Compression-induced nonplanar crack extension with application to splitting, exfoliation, and rockburst. J. Geophys. Res. 87, 6805–6821.
Nemat-Nasser, S., Horii, H., 1993. Micro-Mechanics: Overall Properties of Heterogeneous Materials. North-Holland, Amsterdam.
Paliwal, B., Ramesh, K.T., 2008. An interacting micro-crack damage model for failure of brittle material under compression. J. Mech. Phys. Solids 56, 896–923.
Sanchez-Palencia, E., 1980. Non-homogeneous media and vibration theory. Lecture Notes in Physics, vol. 127. Springer, Berlin.
Schulson, E.M., 2001. Brittle failure of ice. Eng. Fract. Mech. 68, 1839–1887.
Schütte, H., Bruhns, O.T., 2002. On a geometrically nonlinear damage model based on a multiplicative decomposition of the deformation gradient and the propagation of microcracks. J. Mech. Phys. Solids 50, 827–853.
Tada, H., Paris, P.C., Irwin, G.R., 2000. The Stress Analysis of Cracks Handbook. ASME Press, New York.
Voyiadjis, G.Z., Park, T., 1999. The kinematics of damage for finite-strain elasto-plastic solids. Int. J. Eng. 37, 803–830.
Wang, J., Fang, J., Karihaloo, B.L., 2000. Asymptotics of multiple crack interactions and prediction of effective modulus. Int. J. Solids Struct. 37, 4261–4273.
Wang, G.S., 2005. Effective elastic properties of the double-periodically cracked plates. Int. J. Numer. Anal. Meth. Geomech. 29, 1457–1483.
Wiederhorn, S., Bolz, L., 1970. Stress corrosion and static fatigue of glass. J. Am. Ceram. Soc. 53, 543–548.
Zhu, Q., Kondo, D., Shao, J.F., Pensee, V., 2008. Micromechanical modelling of anisotropic damage in brittle rocks and application. Int. J. Rock. Mech. Min. Sci. 45, 467–477.